Journal of Materials Chemistry A

Accepted Manuscript

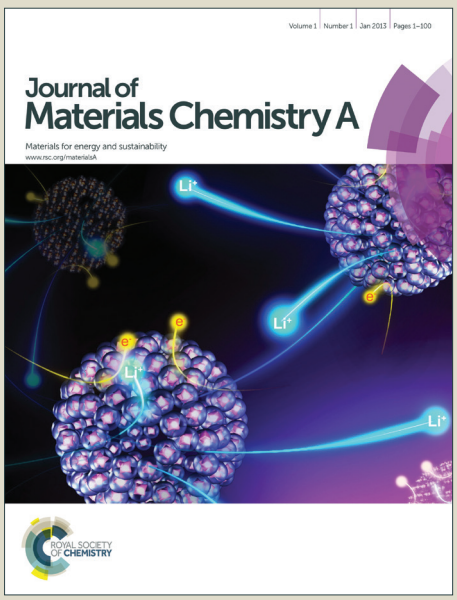

ROYAL SOCIETY OF CHEMISTRY

www.rsc.org/materialsA

Jounal of
Materials Chemistry A

RSCPublishing

ARTICLE

Urchin-like Pd@CuO-Pd Yolk-shell Nanostructures: Synthesis, Characterization and Electrocatalysis

Cite this: DOI: 10.1039/x0xx00000x

Ying Guo[a,b], Yi-Tao Xu[a], Bo Zhao[a, b], Tao Wang[a], Kai Zhang[c], Matthew M. F. Yuen[c], Xian-Zhu Fu[*,a], Rong Sun[*,a], Ching-Ping Wong[d,e]

Received 00th January 2012,
Accepted 00th January 2012

DOI: 10.1039/x0xx00000x

www.rsc.org/

Novel urchin-like Pd@CuO-Pd yolk-shell nanostructures are synthesized through a subsequent oxidizing Pd@Cu_2O truncated octahedron core-shell precursors with $PdCl_4^{2-}$ aqueous solution. The permeable hierarchical CuO shells are constructed by a radially standing 1D single-crystalline nanothorn with Pd nanoparticles. The Pd nanocube cores are encapsulated and confined in the void space of the urchin-like shells. The urchin-like yolk-shell Pd@CuO-Pd nanostructures demonstrate excellent electrocatalytic activity and selectivity for glucose oxidation. Enzyme-free glucose biosensors based on the urchin-like yolk-shell Pd@CuO-Pd electrocatalysts display a higher sensitivity (665.9 μA cm^{-2} mM^{-1}) than that of the CuO nanoparticles (455.8 μA cm^{-2} mM^{-1}), Cu_2O nanoparticles (220.4 μA cm^{-2} mM^{-1}), Pd@Cu_2O truncated octahedrons (179.1 μA cm^{-2} mM^{-1}), Pd mixtures (65.5μA cm^{-2} mM^{-1}) and Pd nanocubes (1.42 μA cm^{-2} mM^{-1}). The outstanding electrocatalytic performance of the urchin-like Pd@CuO-Pd yolk-shell nanostructures might be ascribed to two reasons: the unique hierarchical yolk-shell structures provide highly exposed active sites and act as individualized nanoreactor to enhance the mass diffusion and transport of reactants at electrode/electrolyte interface. Moreover, the nanocomposite of metal oxide semiconductor CuO and noble metal Pd would result in a synergetic effect to improve the electrocatalysis.

Introduction

Design and fabrication of nanocomposites with unique morphologies or structures, such as core-shell and hollow structure, have been of great research efforts for their idiographic physical and chemical properties.[1-5] For example, they could provide powerful platforms for the controlled delivery and medical imaging,[6-9] confined catalysis,[10-12] energy storage and conversion.[13-17] Especially, the yolk-shell or rattle-type nanostructures, with a distinctive core@void@shell configuration consist of a filled core within a single or multiple shell(s),[18-22] are emerging as an interesting family of complex new core-shell or hollow nanostructures.[23,24] Owing to their hierarchical nanostructures and intriguing properties of cores, interstitial hollow spaces, and functionality of shells, yolk-shell architectures are different from single core-shell or hollow structures.[25] In general, the free nanoparticles are prone to aggregate and difficult to handle in catalytic applications. In yolk-shell nanostructure system, the outer shells have been developed to encapsulate and stabilize the metal particles for maintain its compositional and structural integrity,[26] meanwhile, allow for the selective percolation of molecules in and out of the interior of the shell to increase the biocompatibility or promote the catalytic activity to the overall structure.[27] Moreover, the interstitial void inner space between the core and the shell can provide a unique environment to retain specific substances as buffering spaces for interacting with the core nanoparticles and permeable shells. Furthermore, their fabricability and functionality can endow the yolk-shell nanostructures with new properties in catalysis, rendering them attractive for applications as an individualized nanoreactor.[28]

On the other hand, urchin-like hierarchical nanostructures, a quasi-three-dimensional architecture, composed of one- or two-dimensional nanostructures, could greatly improve the performance in electrochemical applications.[29-31] As a result of scattering superstructures effectively reduce the contact area between urchin-like nanostructures, they are not prone to aggregate and exhibit long-term stability, although high specific surface area.[32] Meanwhile, the high-porosity scattering superstructures enable full exposure of the active sites to electrolyte, and provide a short diffusion path for ions or electrons and efficient channels for enhancing the mass diffusion and transport of reactants.[33,34] Thus urchin-like nanostructures have attracted considerable attention in various applications, especially in the catalysis and energy storage and conversion.[35-36]

Electrocatalytic reactions are very important in fuel cells, biosensors, pollution treatment, chemicals production, etc.[2-4,37-39] For example, renewable energy or power for bioelectronics in vivo could be obtained by electrocatalytic oxidation of glucose in bio fuel cells because glucose is the most abundant monosaccharide in the nature and widespread in the blood of living organisms.[3] Moreover, regular detection of glucose is necessary for therapy of diabetes, which also usually based on electrocatalysis of glucose oxidation. A lot of electrocatalysts have been developed for glucose oxidation in recent

[a]*Shenzhen Institutes of Advanced Technology, Chinese Academy of Sciences, Shenzhen, China. E-mail: xz.fu@siat.ac.cn; rong.sun@siat.ac.cn; Fax: +86-755-86392299; Tel: +86-755-86392151*
[b]*Shenzhen College of Advanced Technology, University of Chinese Academy of Sciences, Beijing, China*
[c]*Department of Mechanical Engineering, The Hong Kong University of Science and Technology, Clear Water Bay, Kowloon, Hong Kong, China*
[d]*Department of Electronics Engineering, The Chinese University of Hong Kong, Hong Kong, China*
[e]*School of Materials Science and Engineering, Georgia Institute of Technology, Atlanta, GA 30332, United States*

years.[38,39] Among them, metal oxides, especially Cu oxides, usually demonstrate excellent properties including low cost, high biocompatibility, good anti-poisoning, as well as high catalytic activity, which is far different from noble metal, such as Au, Ag, Pt etc.[6,21,39]

Herein, we design and fabricate novel yolk-shell nanostructures with permeable urchin-like CuO-Pd shells and cubic Pd cores as high performance nanocomposite electrocatalysts for glucose oxidation. Scheme 1 illustrates the synthesis procedure for the urchin-like Pd@CuO-Pd yolk-shell nanostructures. Pd nanocubes are firstly prepared as seeds for deposition of Cu_2O to form Pd@Cu_2O truncated octahedrons precursors. Then the urchin-like Pd@CuO-Pd yolk-shell nanostructures are obtained through treating the Pd@Cu_2O core-shell nanoparticles aqueous suspensions in presence of Na_2PdCl_4 as the assistant agent under a mild temperature. As electrocatalysts, the urchin-like Pd@CuO-Pd yolk-shell nanostructures display much higher activity toward glucose oxidation than both of the Pd@Cu_2O truncated octahedrons and Pd nanocubes. The excellent electrocatalysis might be originated from the novel unique hierarchical urchin-like Pd@CuO-Pd yolk-shell architecture and the synergistic effect of CuO and Pd.

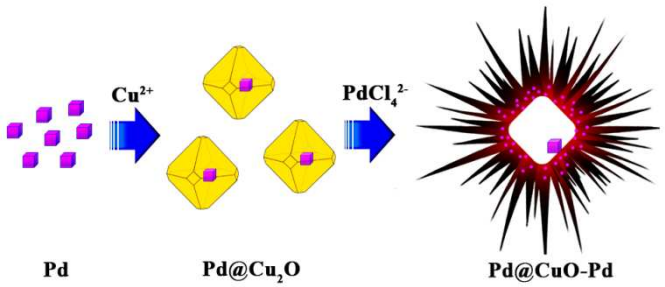

Scheme 1. Synthetic procedure of the urchin-like Pd@CuO-Pd yolk-shell nanostructures.

Experimental

Materials

All chemical reagent are analytical grade and used without further purification. Sodium tetrachloropalladate(II) (Na_2PdCl_4, ≥ 99.9%), copper chloride dehydrate ($CuCl_2·2H_2O$, ≥ 99.0%), hydrazine ($N_2H_4·H_2O$, 85%), L-ascorbic acid ($C_6H_8O_6$, ≥ 99.7%) polyvinylpyrrolidone (PVP, K-30), Sodium dodecyl sulfate (SDS, $C_{12}H_{25}NaO_4S$, ≥ 99.0%), potassium hydroxide (KOH, ≥ 90%), hydrochloric acid (HCl, 37%), glucose ($C_6H_{12}O_6$, ≥ 99.8%), uric acid ($C_5H_4N_4O_3$, ≥ 99.0%), sodium chloride (NaCl, ≥ 99.5%), dopamine hydrochloride ($C_8H_{11}NO_2·HCl$) and L-ascorbic acid ($C_6H_8O_6$, ≥ 99.7%) were purchased from Sinopharm chemical reagent Co., Ltd (Shanghai, China). High purity N_2 was supplied by the Shenzhen Hongzhou Industrial Gases Co., Ltd (Shenzhen, China). Deionized Mini-Q water (18 MΩ cm) was used for all experiments.

Synthesis of Pd Nanocubes

The Pd nanocubes were prepared by modifying the protocol previously reported.[40,41] Briefly, 8 mL of an aqueous solution containing PVP (105 mg), L-ascorbic acid (60 mg) and KBr (600 mg) in a 20-mL vial was heated at 80ºC in air under magnetic stirring for 5 min, and then 3 mL of an aqueous solution containing Na_2PdCl_4 (57 mg) was added with a pipette. After that, the reaction was allowed to continue at 80ºC for 3 h. The nanocubes solution was collected by centrifugation at 15000 rpm for 5 min, washed with deionized water for 3 times and then dispersed in 15 mL water with a concentration of ca. 1.35 mg/mL for elemental Pd.

Synthesis of Pd@Cu_2O Truncated Octahedrons

Firstly, in one 100 mL flask, $CuCl_2·2H_2O$ (0.0426 g) and SDS (0.721 g) were dissolved in 45 mL deionized water. Then 400 μL of Pd nanocubes solution was added and followed by slow addition of 5 mL 2 M NaOH aqueous solution. After stirring in air for 20 min, 5 mL of an aqueous solution of $N_2H_4·2H_2O$ (120 μL, 85%) was added drop-wise into the mixture under vigorous stirring. After 40 min, the obtained solution was centrifuged and washed with deionized water and ethanol 4 times and then dispersed in deionized water (40 mL).

Synthesis of Urchin-like Pd@CuO Yolk-shell Nanostructures

For the preparation of urchin-like Pd@CuO yolk-shell nanostructures, 150 μL of 10 mM Na_2PdCl_4 was added into 40 mL of the Pd@Cu_2O truncated octahedrons colloid solution under vigorous stirring. Then, the mixture was stirred continuously in an oil bath at 90 ºC for 2 h. Finally, the products were collected by centrifuging and washed with deionized water and ethanol 4 times, and then dried in vacuum at 40 °C for 12 hours.

Synthesis of electrocatalysts for activity comparison

The Cu_2O nanoparticles and CuO-removed urchin-like Pd@CuO-Pd yolk-shell nanostructures were prepared for activity comparison.

The synthesis of Cu_2O nanoparticles as follow: A 5 mL of NaOH (2 M) was injected into 50 mL mixed aqueous solution that contained $CuCl_2$ (5 mM) and PVP (0.15 M) under constant stirring at room temperature. After reaction for 30 min, 5 mL 0.5 M AA solution was added into the mixture under constant stirring for 40 min, the final precipitates were extracted from the solution by centrifugation, and then washed with distilled water and ethanol for 5 times, dried in vacuum at 40°C for 4 hours.

The urchin-like Pd@CuO-Pd (25 mg) yolk-shell nanostructures was re-dispersed 50 mL 0.1M HCl solution to remove the CuO for obtaining Pd mixtures.

Characterization

The morphologies and structures of as-synthesized materials were characterized by field emission scanning electron microscopy (FE-SEM, FEI Nova Nano SEM 450) and high resolution transmission electron microscopy (HRTEM, Tecnai G2 F20 FEI), respectively. The X-Ray diffraction (XRD，Rigaku D/Max 2500, Japan) with Cu-Kα radiation was taken to measure the crystallographic structure of the as-prepared samples. The X-Ray diffraction (XRD，Rigaku D/Max 2500, Japan) with Cu-Kα radiation was taken to measure the crystallographic structure of the as-prepared samples. The electrochemical measurements were carried out on electrochemical workstation (CHI 440C, Shanghai, China).

Electrochemical Measurements

The drop-casting films of the synthesized samples on a glassy carbon electrode (GCE, diameter: 5 mm, area: 0.196 cm^2) were used as the working electrode. The Ag/AgCl (3 M KCl, aq) and the platinum-plate electrode (1 cm × 1.5 cm) were served as the reference electrode and the counter electrode, respectively. Prior to electrochemical measurements, the GCE was polished with 50 nm α-Al_2O_3 powder to a high mirror finish and cleansed by sonication. The catalysts inks were prepared by dispersing the as-synthesized

products (4 mg) in ethanol (1 mL) and 0.1 wt % Nafion (1 mL). The dispersion was sonicated for 30 min to form a homogeneous ink. And then as-synthesized samples solution (10 μL) was deposited on the GCE and dried at 40°C. Next, 10 μL 0.1wt% Nafion solution was dropped on the surface of the above catalysts modified CGE and dried at 40°C before electrochemical experiments. The loadings of as-synthesized products on the GCE are 20 μg. All electrochemical measurements were carried out in N_2-saturated 0.1 M KOH solution under room temperature.

Results and discussion

Synthesis and Characterization of Pd@Cu_2O Truncated Octahedrons

As shown in the Scheme 1, Pd@Cu_2O truncated octahedrons are assembled by overgrowth of Cu_2O on the Pd nanocubes. The Pd nanocubes as seeds are firstly fabricated in aqueous solution by reducing Na_2PdCl_4 with L-ascorbic acid and using the KBr and poly(vinylpyrrolidone) (PVP) as the capping agents to promote the formation of (100) facets. As depicted in Figure 1a TEM image, the as-prepared Pd nanoparticles are homogenous and well-dispersed cubes with an average side length of about 15 nm. The Pd@Cu_2O truncated octahedrons are then prepared by growing Cu_2O layer around the 15-nm Pd nanocubes through reduction of Cu^{2+} ions with $N_2H_4{\cdot}H_2O$ in the presence of SDS as capping agents. As shown in Figure 1b SEM image, it is clear that the Pd@Cu_2O nanoparticles exhibit well-shaped octahedral structure with a little truncation and the edge size of Pd@Cu_2O truncated octahedron is ca. 100 nm. From the high-resolution transmission electron (HRTEM) image (Figure 1c), the obvious bright/dark contrast clearly demonstrates the successful fabrication of Pd@Cu_2O core-shell nanostructure. The size of core is line with that of the 15-nm Pd seed. And the thickness of Cu_2O shell is 35±5 nm. The SAED pattern indicates that the Cu_2O shell is single-crystalline. The FFT-generated HRTEM image of a small region of Cu_2O shell exhibits clear lattice fringes separated by 0.24 nm and 0.31 nm, corresponding to the face-centered cubic (fcc) Cu_2O(111) and Cu_2O(110) lattice facets (JCPDS no. 65-3288), respectively. Furthermore, the STEM-EELS mapping confirms the presence and distribution of Cu, O and Pd elements. It is obvious that the signals of Pd are mainly detected in the core region and barely in the shell region, whereas the signals of Cu and O are homogeneous distribution, which further confirm the core-shell truncated octahedral structure (Figure 1d). For the formation of Pd@Cu_2O core-shell nanostructures, the cubic Pd nanoparticles are uniformly dispersed in the Cu^{2+} solution firstly as seeds. During the Cu_2O deposition, the Pd nano-seeds could trigger and guide the growth of Cu_2O shells on the Pd surface with morphological and orientation control, which is similar to the core-shell structured Au@Cu_2O fabrication.[42-44] Thus, Pd@Cu_2O core-shell nanostructures could be obtained and just one Pd nanocube at the centers of the composites.

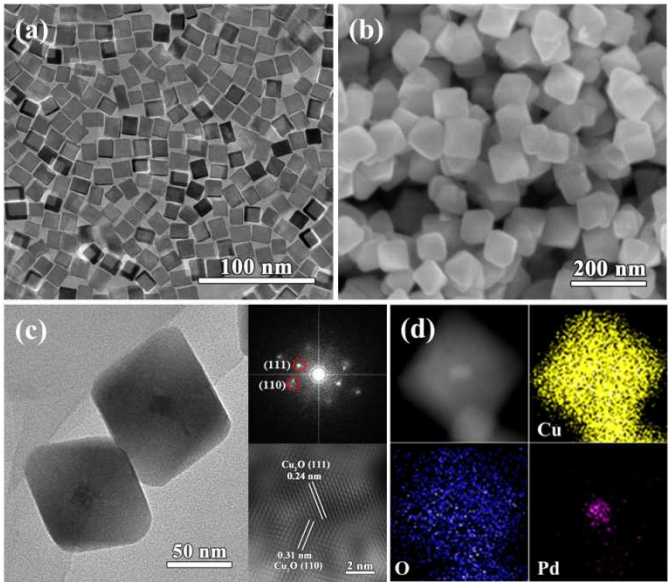

Figure 1. (a) TEM image of the Pd nanocubes. (b) SEM and (c) TEM images of the Pd@Cu_2O truncated octahedrons. Inset: The selected-area electron diffraction (SAED) pattern (up) and FFT-generated HRTEM image (down) of a small region of the Cu_2O shell as indicated. (d) STEM-EELS mapping of the Pd@Cu_2O truncated octahedrons.

Structures and Characterization of Urchin-like Pd@CuO-Pd Yolk-shell Nanostructures

The shape of Cu_2O could easily undergo deformation during pre-treatments or chemical reactions, and very prone to convert into CuO in an oxygen-dissolved aqueous solution due to the low stability of Cu(I).[45,46] To obtain reformatted Cu_2O, the targeted reshaping process in conducted by treating the re-dispersed Pd@Cu_2O aqueous suspensions in presence of Na_2PdCl_4 as the assistant agent under a mild temperature of 90ºC for 2 h. Figures 2a-c show the representative SEM images of the heat-treated Pd@Cu_2O truncated octahedrons with different magnifications. The original shape of Pd@Cu_2O truncated octahedron is severely deformed after heat treatment. The surface is very different from the initial surface of Pd@Cu_2O truncated octahedron and becomes very rough. Radially standing 1D nanothorns with an average length size of 50-150 nm are observed, and grown onto the particles to assemble an urchin-like hierarchical structure. The interior structure is further observed by TEM, as shown in Figures 2d, e. The permeable shell is constructed by radial nanothorns with an average diameter and length size of 10-15 nm and 50-150 nm, respectively, in good line with the SEM results. The higher magnification TEM image in Figure 2d clearly illustrates the typical Pd@CuO-Pd urchin-like yolk-shell nanostructures. The cubic Pd core still maintains in the interior but no in the center while with large void when the initial solid Cu_2O shell are instead of the special shells with radial nanothorns after heat treatment.

Figure 2i shows the corresponding Cu, O and Pd STEM-EELS mapping of the urchin-like Pd@CuO-Pd yolk-shell nanostructure. The Pd is distributed in the yolk and the shell region within the entire 3D structure. The Pd on the shell is stemmed from Na_2PdCl_4 assistant agent for the Cu_2O reduction of Pd^{2+} to form CuO thorns during the heat treatment. The Pd/Cu atomic ratio increases from 1.7/98.3 to 4.1/95.9 (Figure S1, Supporting Information). The Cu and O elements are distributed uniformly around the Pd core. These results further demonstrate that the obtained material forms rattle-type superstructure with permeable CuO shell and cubic Pd core. The Figure 2f displays the HRTEM image of cubic Pd core. The fringes with lattice spacing of 0.338 nm and 0.224 nm can be indexed to the face-centered cubic (fcc) Pd (100) and (111) lattice facets, respectively. The crystal plane angle of Pd (100) and (111) is 54.7º (JCPDS no. 65-2867). Figure 2g gives the HRTEM image of the root region of nanothorn, clearly illustrating the presence of two sets of lattice fringes. Corresponding to the monoclinic CuO (200) and (002) lattice

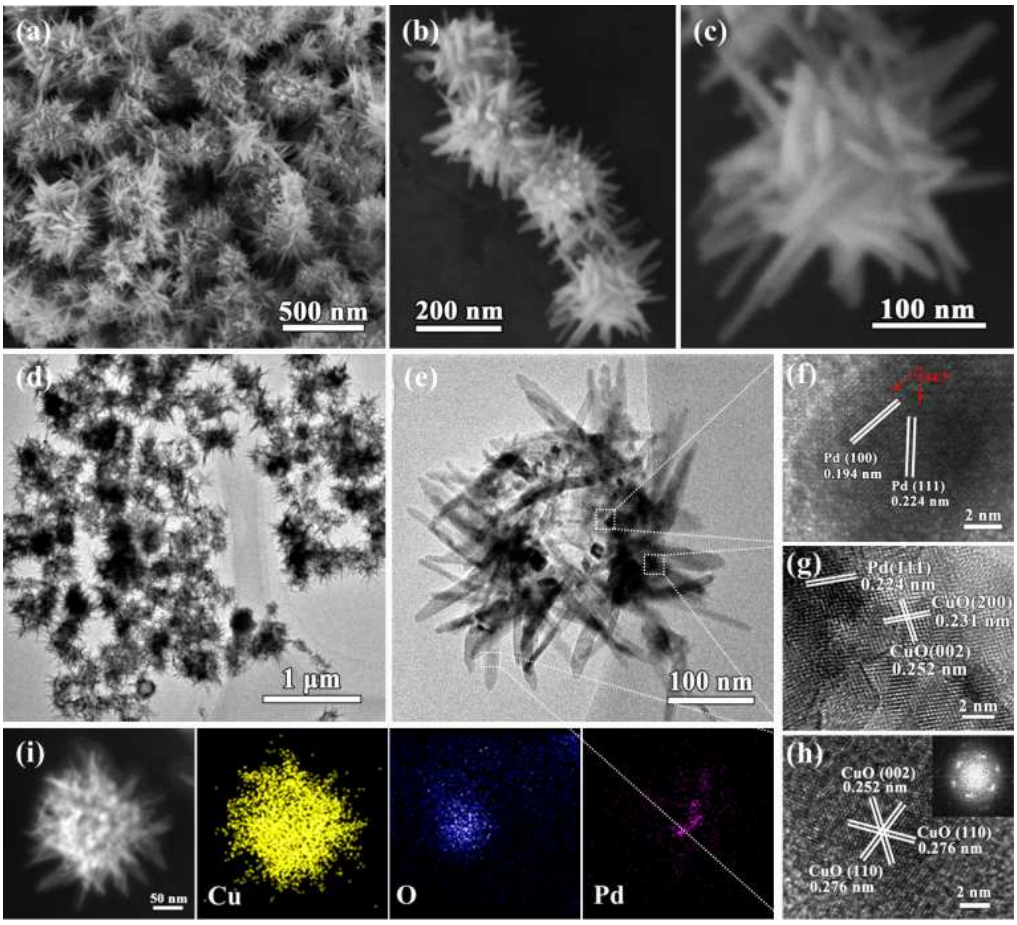

Figure 2. (a-c) SEM images of the urchin-like Pd@CuO-Pd yolk-shell nanocompositions. (d-h) TEM and HRTEM images of the urchin-like Pd@CuO-Pd yolk-shell nanocompositions. (i) STEM-EELS mapping of the Pd@CuO-Pd nanostructures.

facets, the lattice spacing is 0.231 nm and 0.252 nm, respectively (JCPDS no. 45-0937). And the lattice fringes of Pd also are observed in root region, indicating that the interplanar distances is 0.224 nm for the Pd (111) crystal planes, which could be generated from Pd deposition reaction by oxidative etching Cu_2O shell with Na_2PdCl_4 assistant agent. It is worth noting that the single urchin-like yolk-shell nanostructures reveal a polycrystalline nature because of radial orientation of nanothorns (Figure S2, Supporting Information). However, each nanothorn exhibits the single-crystalline feature and possesses the lattice fringes of CuO (002) and (110) lattice facets with an interplanar spacing of 0.252 nm and 0.276 nm (Figure 2h), respectively.

Oxidation of Cu_2O easily occurs to form the more thermodynamically stable CuO with morphology deformation in neutral aqueous solution by heating treatment with assistant agents.[45,46] The plausible formation reactions that are involved in growth of urchin-like hierarchical structures in presence of Na_2PdCl_4 assistant agents under heat treatments are suggested as follow: [47]

$$PdCl_4^{2-} + Cu_2O + H_2O \rightarrow Pd + 4Cl^- + 2CuO + 2H^+ \quad (1)$$
$$2Cu_2O + O_2 + 8H^+ \rightarrow 4Cu^{2+} + 4H_2O \quad (2)$$
$$4Cu^{2+} + 2H_2O \rightarrow 4CuO + 8H^+ \quad (3)$$

Initially, the $PdCl_4^{2-}$ is reduced on the surface of Cu_2O shells of Pd@Cu_2O truncated octahedrons, and Cu(I) offers the electrons after being transformed into Cu(II) by galvanic replacement (reaction 1).

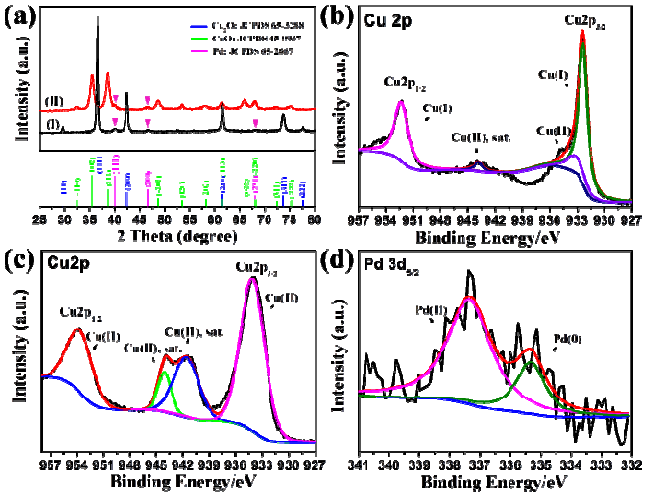

Figure 3. (a) XRD patterns of as-synthesized products: (I) The Pd@Cu_2O truncated octahedrons and (II) The urchin-like Pd@CuO-Pd yolk-shell nanostructures. The high-resolution XPS spectra of the as-prepared materials: (b) Cu 2p spectrum of the Pd@Cu_2O truncated octahedrons. (c) Cu 2p and (d) Pd 3d spectrum of the urchin-like Pd@CuO-Pd yolk-shell nanostructures.

Then, the H^+ served as catalysts to facilitate Cu_2O dissolution and CuO formation (reaction 2 and 3). It is noteworthy that the reactions should be carried out in air, because dioxygen behaves as real oxidatant of Cu(I) to Cu(II). Besides, the heating treatment expedites the transformation from Cu_2O to CuO. Eventually, thermodynamically stable CuO is produced and reshaped to urchin-like Pd@CuO-Pd yolk-shell nanostructures since the cubic Pd cores still remain inside.

XRD patterns (I) in Figure 3a show strong reflection peaks for cubic crystal structure of Cu_2O (JCPDS no. 65-3288). Furthermore, there are weak Pd diffraction peaks indicated by pink triangle in the XRD patterns (I), resulting from the core-shell nature of the Pd@Cu_2O truncated octahedrons. The strong Cu_2O diffraction peaks transfer into monoclinic CuO reflected peaks after heating treatment in the XRD patterns (II). The weak diffraction peaks of Pd still could be detected at 40.1º, 46.7º and 68.2º, corresponding to the Pd(111), (200) and (220) planes, respectively (JCPDS no. 65-2867). The surface element composition and chemical state of the as-prepared materials are also investigated by XPS measurements (Figure 3b-c). According to the high-resolution spectrum of the Pd@Cu_2O truncated octahedrons (Figure 3b), Cu 2p1/2 and Cu 2p3/2 peaks at 952.3 eV and 932.4 eV are ascribed to Cu(I).[48] In addition, the weaker and shake-up peaks at 933.4 eV and 943.8 eV are characteristic of Cu(II).[49] The result indicates that the surface of Pd@Cu_2O truncated octahedrons is slightly oxidized due to the low stability of Cu_2O. After heating treatment, the mainly peaks of Cu(I) generally shift to high binding energy for Cu(II) (Figure 3c). The typical Cu 2p1/2 and 2p3/2 peaks of Cu(II) with two shake-up satellites (denoted as "sat.") are obtained at 953.9 eV and 934.1 eV,[50] respectively. Moreover, the two asymmetric peaks are observed at 335.4 eV and 337.4 eV for the Pd3d spectrum and are assigned to Pd(0) and Pd(II), as shown in Figure 3d. It suggests that the Pd(II) is rich on the surface of Pd, which might be resulted from the interface charge interaction between the metal oxide semiconductor CuO and noble metal Pd.

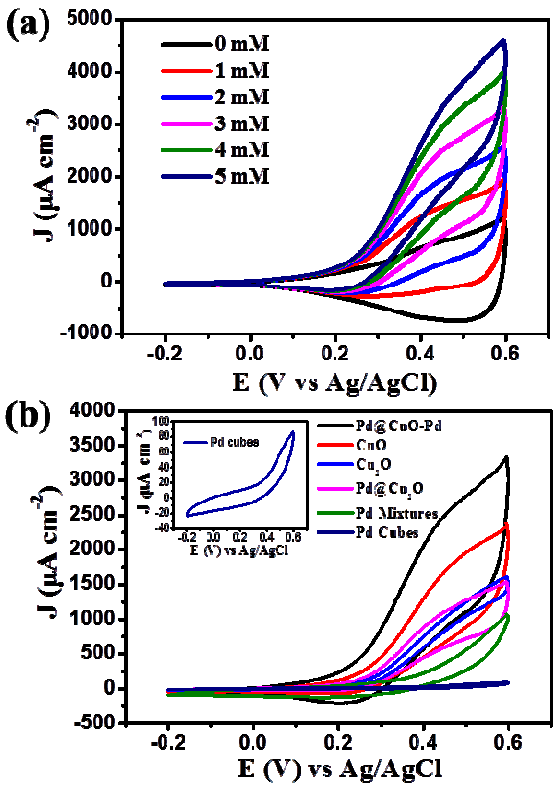

Figure 4. (a) CV curves of the urchin-like Pd@CuO-Pd yolk-shell nanostructures in a series of glucose in N_2-saturated 0.1 M KOH solution at a scan rate of 100 mV s^{-1}. (b) CV curves of the Pd nanocubes (black line), the Pd@Cu_2O truncated octahedrons (blue line) and the urchin-like Pd@CuO-Pd yolk-shell nanostructures (red line) in N_2-saturated 0.1 M KOH solution with the presence of 4 mM glucose at a scan rate of 100 mV s^{-1}.

Electrochemical Catalysis toward Glucose Oxidation

Electrochemical catalytic activity of the urchin-like Pd@CuO-Pd yolk-shell nanostructures is investigated by cyclic voltammogram technique. Figure 4a displays the cyclic voltammograms (CVs) over a voltage range from -0.2 to 0.6 V for the urchin-like Pd@CuO-Pd yolk-shell nanostructures electrode in 0.1 M KOH solution with different glucose concentration at a sweep rate of 100 mV s^{-1}. The oxidation currents at ca. 0.41 V obviously increase as introduction of glucose compared to that without glucose, indicating the electrochemical oxidation of glucose over the urchin-like Pd@CuO-Pd yolk-shell nanostructures electrode. And the peak current is enlarged with the increasing glucose concentration since the more electrons could be provided with high content of reaction reagents during electrochemical oxidation.[51] Figure 4b presents the CV curves of different electrodes in 0.1 M KOH solution with 3 mM glucose at a scan rate of 100 mV s^{-1}. The oxidation current of Pd nanocubes is the lowest, and improved for the hollow Pd nanoparticles and Pd mixtures obtained by etching CuO in the urchin-like Pd@CuO-Pd yolk-shell nanostructures due to the enhancement of electrocatalytic activity from smaller particle size and larger surface area (Figure S5 and S7). The oxidation currents of these Pd nanoparticles are less than those of CuO, Cu_2O nanoparticles although the sizes of CuO and Cu_2O nanoparticles (Figure S5 and S4) are larger than those of Pd nanoparticles. The results reveal that Cu_2O and CuO nanoparticles possess higher electrocatalytic activity than Pd nanoparticles towards glucose oxidation. Comparing to Pd@Cu_2O truncated octahedrons, the pure Cu_2O nanoparticles exhibit oxidation current as similar as those of Pd@Cu_2O truncated octahedrons toward glucose oxidation, indicating that the core Pd nanocubes of Pd@Cu_2O truncated octahedrons do not improve the electrochemical activity due to over-thick Cu_2O shells. The oxidation current of the CuO nanoparticles are slightly larger than those of the pure Cu_2O nanoparticles and Pd@Cu_2O truncated octahedrons, but lower than that of the urchin-like Pd@CuO-Pd yolk-shell nanostructures, suggesting that metal Pd not only enhance the electrocatalytic activity of the urchin-like Pd@CuO-Pd yolk-shell nanostructures, but also facilitate the reshaping process of urchin-like superstructures.[48] The urchin-like Pd@CuO-Pd yolk-shell nanostructures exhibit remarkably larger oxidation currents than the Pd nancubes, Pd mixtures, hollow Pd nanoparticles, Cu_2O nanoparticles, CuO nanoparticles, and Pd@Cu_2O truncated octahedrons. It indicates much higher electrocatalytic activity of urchin-like Pd@CuO-Pd yolk-shell nanostructures relative to these electrocatalysts for comparison. The outstanding electrocatalysis of urchin-like Pd@CuO-Pd yolk-shell nanostructures might be originated from their unique permeable urchin-like and yolk-shell superstructure, which could supply more exposed reaction active sites and lots of channels facilitating the mass diffusion and transport of reactants at electrode/electrolyte interface, and serves as

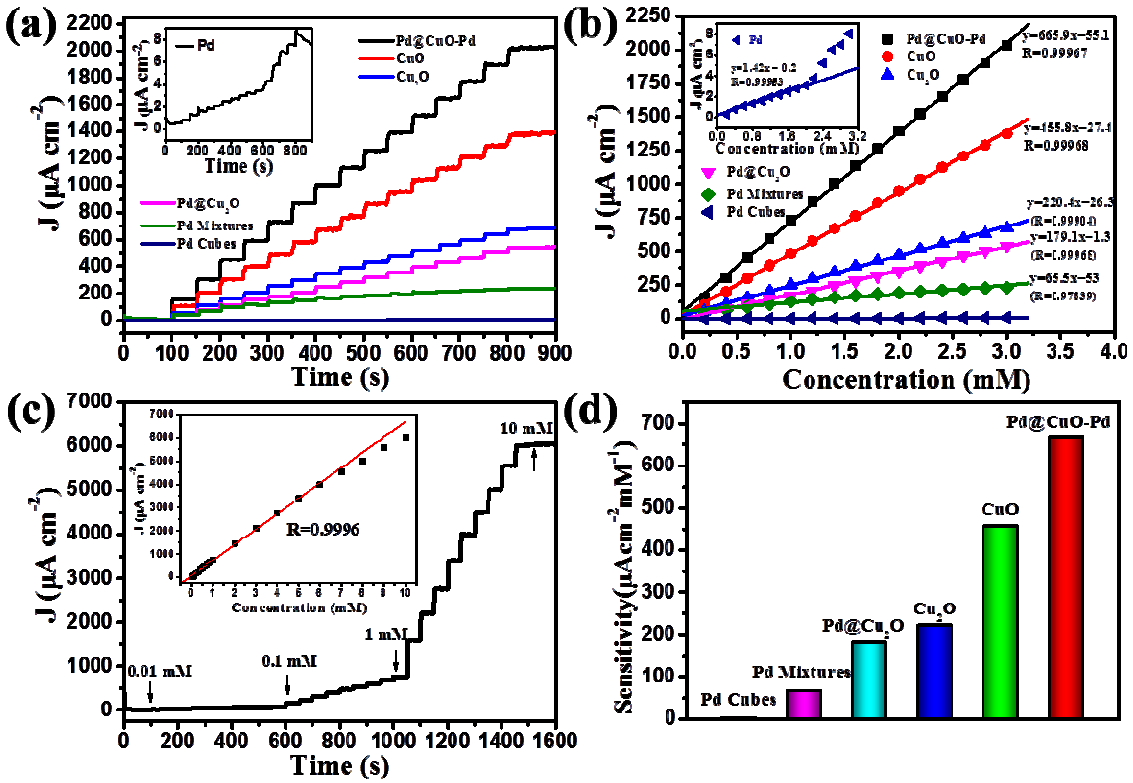

Figure 5. (a) Amperometric responses curves and (b) the corresponding calibration curves of the as-prepared electrocatalysts upon successive addition of glucose in N_2-saturated 0.1 M KOH at 0.5 V (vs Ag/AgCl). (c) Amperometric response of the urchin-like Pd@CuO-Pd yolk-shell nanostructures after successive addition of glucose in N_2-saturated 0.1 M KOH at 0.5 V (vs Ag/AgCl). Inset: calibration curve for the amperometric response. (d) The corresponding sensitivities of the as-prepared biosensors at potential of 0.5 V (vs Ag/AgCl).

individualized nanoreactor for glucose molecule delivery systems enabling proper loading with guest glucose molecules toward oxidation. Furthermore, there are intimate interface and charge interaction between of CuO and Pd according to the HRTEM and XPS results, which would lead to synergetic effect to improve the catalytic activity like other reports about composite catalysts of metal oxide semiconductor and noble metal.[52,53]

The glucose oxidation reaction occurring at Cu-based catalyst electrode surface in alkaline solution could be ascribed to Cu(II) and Cu(III) surface species as shown in the following:[54]

$$CuO + OH^- \rightarrow CuOOH + e \quad (4)$$

$$CuOOH + \text{glucose} + e \rightarrow \text{gluconolactone} + CuO + OH^- \quad (5)$$

$$\text{Gluconolactone} \rightarrow \text{gluconic acid} \quad (6)$$

During the electrocatalysis, the CuO on the electrode surface would be firstly oxidized into CuOOH (reaction 4) at a certain potential, and the oxidation-generated CuOOH then service as an electron-transfer medium to catalyze glucose oxidation to form gluconolactone (reaction 5),[55] and the gluconolactone would be further oxidized into gluconic acid(reaction 6). The introduction of Pd could be conducive to expedite electron transfer between noble metal Pd and semiconductor CuO, thus resulting in synergistic effect of the urchin-like Pd@CuO-Pd yolk-shell nanostructures to enhance electrocatalytic activity for glucose oxidation.[48,52,56,57]

Electrocatalytic oxidation of glucose could be applied in biosensors. To evaluate the sensitivity of biosensors based on the as-prepared electrocatalysts, the chronoamperometry is performed. Figure 5a depicts the amperometric response curves of glassy carbon (GC) electrodes modified with different electrocatalysts upon the successive addition of glucose at 0.5 V vs Ag/AgCl electrode. The currents increase immediately with increases in the glucose concentrations, and quickly reach the steady-state and they display a fast response time (less than 3 s, reaching about 95% of steady-state current), indicating the sensitive and rapid responses of the urchin-like Pd@CuO-Pd yolk-shell nanostructures and Pd@Cu_2O truncated octahedrons toward glucose monitor. And the largest current response of the urchin-like Pd@CuO-Pd yolk-shell nanostructures toward glucose sensing is obviously recorded. Figure 5b displays the linear relationship between the current density and the glucose concentrations. Both of urchin-like Pd@CuO-Pd yolk-shell nanostructures and Pd@Cu_2O truncated octahedrons present good linear response to the change of glucose concentration in the range of 0.2-3 mM. The Pd nanocubes, however, exhibit linear relationship in the range only of 0.2-2.0 mM. The sensitivity of the biosensors could be calculated from the linear regression equations (Figure 5b). The sensitivity of the urchin-like Pd@CuO-Pd yolk-shell nanostructures is up to 665.9 μA cm^{-2} mM^{-1} for glucose detection, which is 1.46, 3.0, 3.7, 10.2 and 468.9 times as high as that of the CuO nanoparticles (455.8 μA cm^{-2} mM^{-1}), Cu_2O nanoparticles (220.4 μA cm^{-2} mM^{-1}), Pd@Cu_2O truncated octahedrons (179.1 μA cm^{-2} mM^{-1}), Pd mixtures (65.5μA cm^{-2} mM^{-1}) and Pd nanocubes (1.42 μA cm^{-2}

mM^{-1}), respectively. The higher sensitivity of the urchin-like Pd@CuO-Pd yolk-shell nanostructures results from the extremely higher electrocatalytic activity. Moreover, the limits of detection are also can be calculated to be 4 μM for the urchin-like Pd@CuO-Pd yolk-shell nanostructures, in the linear concentration range based on the equation S/N=3. Figure 5c shows a typical wide-range current response curve of the urchin-like Pd@CuO-Pd yolk-shell nanostructures. The linear relationship is good line with Figure 5b. The inset in Figure 5c shows the plot of the current as a function of glucose concentration. The steady-state current of the biosensor is linearly related to the amount of glucose within the concentration range of 0.01-6 mM with a correlation coefficient of 0.9996. The urchin-like Pd@CuO-Pd yolk-shell nanostructures for glucose oxidation are superior for excellent sensitivity, short response time, low detection limit and large linear range relative to the Pd nancubes, Pd mixtures, hollow Pd nanoparticles, Cu_2O nanoparticles, CuO nanoparticles, and Pd@Cu_2O truncated octahedrons. Compared to the other reported electrocatalysts listed in Table S1, the urchin-like Pd@CuO-Pd yolk-shell nanostructures also illustrate excellent performance as glucose biosensors.

The selectivity is an important factor to comment the electrocatalysis. The glucose monitor might be interfered by coexistence interferents with glucose in human blood serum, such as ascorbic acid (AA), dopamine (DA), uric acid (UA) and NaCl.[38] The sensing selectivity of biosensors based on urchin-like Pd@CuO-Pd yolk-shell nanostructures is investigated by introduction of interferents one by one during the glucose sensing process at different potential (Figure 6a). The obvious current responses are recorded after the addition of 1 mM glucose and slight or no signal change can be observed with the subsequent addition of AA, DA, UA and NaCl. The current change at lower potentials (0.4 V) can be neglected comparing to change from glucose oxidation. At three different potentials, the current response from the interferents is below 2.2%. Moreover, there is no further obvious effect on the current of glucose oxidation after the addition of NaCl, indicating that the biosensor possesses excellent selectivity and high chloride tolerance to glucose. It might be resulted from that the most of electroactive interferences in the blood do not show noticeable response currents at lower potential for glucose oxidation of urchin-like Pd@CuO-Pd yolk-shell nanostructures, and unique permeable urchin-like shells increase the surface roughness.[57]

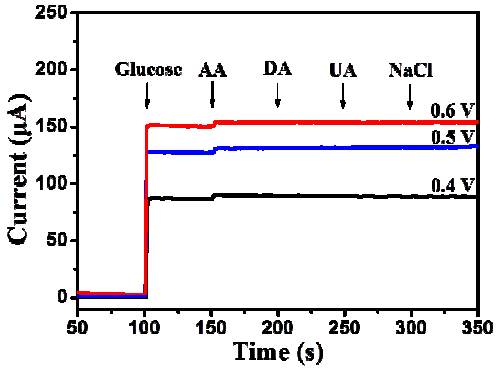

Figure 6. Amperometric response of the biosensor to successive additions of 1 mM glucose, 0.1 mM interferents in N_2-saturated 0.1 M KOH solution at potential of 0.4 V, 0.5 V and 0.6 V (vs Ag/AgCl)

Conclusion

The core-shell Pd@Cu_2O truncated octahedrons are successfully synthesized by using Pdnanocubes as the structures-directing cores for the uniform grown of Cu_2O shells. Subsequently, the Pd@Cu_2O truncated octahedrons are converted to urchin-like Pd@CuO-Pd yolk-shell nanostructures through reshaping process, by heated treatment under mild temperature of 90ºC in aqueous solution. The urchin-like Pd@CuO-Pd yolk-shell nanostructures exhibit much higher electrocatalysis toward glucose oxidation compared to the Pd nancubes, Pd mixtures, hollow Pd nanoparticles, Cu_2O nanoparticles, CuO nanoparticles, and Pd@Cu_2O truncated octahedrons. The biosensors based on urchin-like Pd@CuO-Pd yolk-shell electrocatalysts exhibit superior electrochemical activities with ultrahigh sensitivity, fast response, wide linear range, low detection limit, excellent selectivity and tolerance to Cl^- ions.

Acknowledgements

This work was financially supported by National Natural Science Foundation of China (No.21203236), Guangdong and Shenzhen Innovative Research Team Program (No.2011D052, KYPT20121228160843692), Shenzhen Electronic Packaging Materials Engineering Laboratory (2012-372), Shenzhen High Density Electronic Packaging and Device Assembly Key Laboratory (ZDSYS20140509174237196).

Notes and references

1. G. Chen, Y. Zhao, G. Fu, P. N. Duchesne, L. Gu, Y. Zheng, X. Weng, M. Chen, P. Zhang, C. W. Pao, J. F. Lee and N. Zheng, *Science*, 2014, **344**, 495-499.
2. J. Liu, S. Z. Qiao, J. S. Chen, X. W. Lou, X. Xing and G. Q. Lu, *Chem. Commun.*, 2011, **47**, 12578-12591.
3. X. Xia, Y. Wang, A. Ruditskiy and Y. Xia, *Adv. Mater.*, 2013, **25**, 6313-6333.
4. G. Li and Z. Tang, *Nanoscale*, 2014, **6**, 3995-4011.
5. G. Fu, Z. Liu, Y. Chen, J. Lin, Y. Tang and T. Lu, *Nano Res.*, 2014, **7**, 1205-1214.
6. J. Gao, G. Liang, B. Zhang, Y. Kuang, X. Zhang and B. Xu, *J. Am. Chem. Soc.*, 2007, **129**, 1428-1433.
7. J. Gao, G. Liang, J. S. Cheung, Y. Pan, Y. Kuang, F. Zhao, B. Zhang, X. Zhang, E. X. Wu and B. Xu, *J. Am. Chem. Soc.*, 2008, **130**, 11828-11833.
8. J. Liu, S. Z. Qiao, S. Budi Hartono and G. Q. Lu, *Angew. Chem. Int. Ed.*, 2010, **122**, 5101-5105.
9. X. Zhou, W. Xu, Y. Wang, Q. Kuang, Y. Shi, L. Zhong and Q. Zhang, *J. Phys. Chem. C*, 2010, **114**, 19607-19613.
10. J. H. Pan, Q. Wang and D. W. Bahnemann, *Catal. Today*, 2014, **230**, 197-204.
11. S. Wu, J. Dzubiella, J. Kaiser, M. Drechsler, X. Guo, M. Ballauff and Y. Lu, *Angew. Chem. Int. Ed.*, 2012, **51**, 2229-2233.
12. Z. Li, L. Mo, Y. Kathiraser and S. Kawi, *ACS Catal.*, 2014, **4**, 1526-1536.
13. G. Zhang and X. W. Lou, *Angew. Chem. Int. Ed.*, 2014, **126**, 9187-9190.
14. W. Tian, X. Wang, C. Zhi, T. Zhai, D. Liu, C. Zhang, D. Golberg and Y. Bando, *Nano Energy*, 2013, **2**, 754-763.
15. X. Zhang, X. Song, S. Gao, Y. Xu, X. Cheng, H. Zhao and L. Huo, *J. Mater. Chem. A*, 2013, **1**, 6858-6864.

16. P. Yang, X. Xiao, Y. Li, Y. Ding, P. Qiang, X. Tan, W. Mai, Z. Lin, W. Wu, T. Li, H. Jin, P. Liu, J. Zhou, C. P. Wong and Z. L. Wang, *ACS Nano.*, 2013, **7**, 2617-2626.
17. G. Zhang, H. B. Wu, T. Song, U. Paik and X. W. Lou, *Angew. Chem. Int. Ed.*, 2014, **53**, 12590-12593.
18. K. Kamata, Y. Lu and Y. Xia, *J. Am. Chem. Soc.*, 2003, **125**, 2384-2385.
19. J. Liu, H. Q. Yang, F. Kleitz, Z. G. Chen, T. Yang, E. Strounina, G. Q. Lu and S. Z. Qiao, *Adv. Funct. Mater.*, 2012, **22**, 591-599.
20. W. Meng, W. Chen, L. Zhao, Y. Huang, M. Zhu, Y. Huang, Y. Fu, F. Geng, J. Yu, X. Chen and C. Zhi, *Nano Energy*, 2014, **8**, 133-140.
21. J. Han, R. Chen, M. Wang, S. Lu and R. Guo, *Chem. Commun.*, 2013, **49**, 11566-11568.
22. C.H. Kuo, Y. Tang, L.Y. Chou, B. T. Sneed, C. N. Brodsky, Z. Zhao and C.K. Tsung, *J. Am. Chem. Soc.*, 2012, **134**, 14345-14348.
23. Q. Fang, S. Xuan, W. Jiang and X. Gong, *Adv. Funct. Mater.*, 2011, **21**, 1902-1909.
24. Y. J. Hong, M. Y. Son, B. K. Park and Y. C. Kang, *Small*, 2013, **9**, 2224-2227.
25. Y. N. Ko, Y. C. Kang and S. B. Park, *Chem. Commun.*, 2013, **49**, 3884-3886.
26. C. Chen, X. Fang, B. Wu, L. Huang and N. Zheng, *Chemcatchem*, 2012, **4**, 1578-1586.
27. Z. Teng, S. Wang, X. Su, G. Chen, Y. Liu, Z. Luo, W. Luo, Y. Tang, H. Ju, D. Zhao and G. Lu, *Adv. Mater.*, 2014, **26**, 3741-3747.
28. Y. Yang, X. Liu, X. Li, J. Zhao, S. Bai, J. Liu and Q. Yang, *Angew. Chem. Int. Ed.*, 2012, **124**, 9298-9302.
29. J. H. Pan, X. Z. Wang, Q. Huang, C. Shen, Z. Y. Koh, Q. Wang, A. Engel and D. W. Bahnemann, *Adv. Funct. Mater.*, 2014, **24**, 95-104.
30. Y. Huang, J. Tao, W. Meng, M. Zhu, Y. Huang, Y. Fu, Y. Gao and C. Zhi, *Nano Energy*, 2015, **11**, 518-525.
31. B. Wang, H. Wu, L. Yu, R. Xu, T. T. Lim and X. W. Lou, *Adv. Mater.*, 2012, **24**, 1111-1116.
32. X. He, C. Yue, Y. Zang, J. Yin, S. Sun, J. Li and J. Kang, *J. Mater. Chem. A*, 2013, **1**, 15010-15015.
33. B. Wang, H. Wu, L. Yu, R. Xu, T. T. Lim and X. W. Lou, *Adv. Mater.*, 2012, **24**, 1111-1116.
34. Y. Xiao, S. Liu, F. Li, A. Zhang, J. Zhao, S. Fang and D. Jia, *Adv. Funct. Mater.*, 2012, **22**, 4052-4059.
35. S. W. Chou, H. C. Chen, Z. Zhang, W. H. Tseng, C. I. Wu, Y. Y. Yang, C. Y. Lin and P. T. Chou, *Chem. Mater.*, 2014, **26**, 7029-7038.
36. J. H. Pan, H. Dou, Z. Xiong, C. Xu, J. Ma and X. S. Zhao, *J. Mater. Chem.*, 2010, **20**, 4512-4528.
37. S. C. Sahu, A. K. Samantara, A. Dash, R. R. Juluri, R. K. Sahu, B. K. Mishra and B. K. Jena, *Nano Res.*, 2013, **6**, 635-643.
38. L.C. Jiang and W.D. Zhang, *Biosens. Bioelectron.*, 2010, **25**, 1402-1407.
39. N. Meir, I. J. L. Plante, K. Flomin, E. Chockler, B. Moshofsky, M. Diab, M. Volokh and T. Mokari, *J. Mater. Chem. A*, 2013, **1**, 1763-1769.
40. M. Jin, H. Zhang, Z. Xie and Y. Xia, *Angew. Chem. Int. Ed.*, 2011, **50**, 7850-7854.
41. G. Li, H. Kobayashi, J. M. Taylor, R. Ikeda, Y. Kubota, K. Kato, M. Takata, T. Yamamoto, S. Toh, S. Matsumura and H. Kitagawa, *Nat. Mater.*, 2014, **13**, 802-806.
42. M. Liu, R. Liu and W. Chen, *Biosens. Bioelectron.*, 2013, **45**, 206-212.
43. C. H. Kuo, T. E. Hua and M. H. Huang, *J. Am. Chem. Soc.*, 2009, **131**, 17871-17878.
44. L. Kong, W. Chen, D. Ma, Y. Yang, S. Liu and S. Huang, *J. Mater. Chem.*, 2012, **22**, 719-724.
45. J. C. Park, J. Kim, H. Kwon and H. Song, *Adv. Mater.*, 2009, **21**, 803-807.
46. Q. Hua, K. Chen, S. Chang, Y. Ma and W. Huang, *J. Phys. Chem. C*, 2011, **115**, 20618-20627.
47. J. Kim, Y. Kwon and H. Lee, *J. Mater. Chem. A*, 2013, **1**, 14183-14188.
48. L. Li, X. Chen, Y. Wu, D. Wang, Q. Peng, G. Zhou and Y. Li, *Angew. Chem. Int. Ed.*, 2013, **125**, 11255-11259.
49. D. A. Svintsitskiy, T. Y. Kardash, O. A. Stonkus, E. M. Slavinskaya, A. I. Stadnichenko, S. V. Koscheev, A. P. Chupakhin and A. I. Boronin, *J. Phys. Chem. C*, 2013, **117**, 14588-14599.
50. L. Martin, H. Martinez, D. Poinot, B. Pecquenard and F. Le Cras, *J. Phys. Chem. C*, 2013, **117**, 4421-4430.
51. X. C. Dong, H. Xu, X. W. Wang, Y. X. Huang, M. B. Chan Park, H. Zhang, L. H. Wang, W. Huang and P. Chen, *ACS Nano*, 2012, **6**, 3206-3213.
52. L. Wang, J. Ge, A. Wang, M. Deng, X. Wang, S. Bai, R. Li, J. Jiang, Q. Zhang, Y. Luo and Y. Xiong, *Angew. Chem. Int. Ed.*, 2014, **53**, 5107-5111.
53. Y. Yamada, C. K. Tsung, W. Huang, Z. Huo, S. E. Habas, T. Soejima, C. E. Aliaga, G. A. Somorjai and P. Yang, *Nat. Chem.*, 2011, **3**, 372-376.
54. J. M. Marioli and T. Kuwana, *Electrochim. Acta*, 1992, **37**, 1187-1197.
55. X. Kang, Z. Mai, X. Zou, P. Cai and J. Mo, *Anal. Biochem.*, 2007, **363**, 143-150.
56. S. Bai, J. Ge, L. Wang, M. Gong, M. Deng, Q. Kong, L. Song, J. Jiang, Q. Zhang, Y. Luo, Y. Xie and Y. Xiong, *Adv. Mater.,* 2014, **26**, 5689-5695.
57. K. K. Lee, W. S. Chin and C. H. Sow, *J. Mater. Chem. A*, 2014, **2**, 17212-17248.

Highlighting

Novel urchin-like Pd@CuO-Pd yolk-shell nanostructures derived from Pd@Cu_2O core-shell truncated octahedrons demonstrate excellent electrocatalytic activity and selectivity toward glucose oxidation.